Optical tracking of fiducial markers in the design of a surgical navigation system

Darin Tsui*, Mitsuhiro Jo*, Bryan Nguyen*, Farshad Ahadian** and Frank E. Talke*
*University of California: San Diego, Center for Memory and Recording Research
9500 Gilman Drive, La Jolla, CA 92093, United States
E-mail: ftalke@ucsd.edu
**University of California: San Diego Medical Center
3350 La Jolla Village Drive, San Diego, CA 92161, United States
E-mail: fahadian@health.ucsd.edu

Abstract
Low back pain is the leading cause of non-fatal health loss and years lived with disability. Current interventional pain management therapies include epidural steroid injections and radiofrequency ablations, which can provide short-term and long-term relief. However, these therapies often utilize fluoroscopy, which exposes both the patient and medical practitioner to radiation. In this study, we explore whether an augmented reality navigation (AR) system can be interfaced with a preoperative image from magnetic resonance imaging (MRI) to reduce radiation exposure, provide a low-cost alternative to existing technologies, and improve needle position tracking. Non-invasive skin markers (ArUco) were utilized to identify the surgical field. An XYZ tracking platform with linear Kalman filtering was used to test the feasibility of a marker tracking algorithm. Future studies will address the development of a three-dimensional (3D) marker tracking system, the implementation of optimal ArUco marker materials, and ways to improve marker position accuracy.

Keywords: Augmented reality, Image-guided surgery, Fiducial markers, Navigation system, Marker tracking, Kalman filter, Magnetic resonance imaging

1. Introduction

1.1 Purpose

Eighty percent of all adults experience low back pain in their lifetime (Sizer, et al., 2000). In 2017 alone, 577 million individuals suffered from back pain (James, et al., 2018), with the highest prevalence in those aged 40-80 years (Manchikanti, et al., 2014).

Back pain is the leading cause of non-fatal health loss and disability globally (James, et al., 2018). Increases in obesity, physical inactivity, and an aging population have been attributed to an increase in the pervasiveness of chronic back pain (Battié, et al., 1995; Manchikanti, et al., 2014; Sizer, et al., 2000). Causes for back pain also include genetics and psychological conditions (Kovacs, et al., 2008; Croft, et al., 1995; Truchon, et al., 2008; Currie and Wang, 2005). One of the main consequences of back pain is socio-economic loss, including loss of physical and mental activity, inability to perform in occupational roles, financial burden, and relation strain (Walker, et al., 2006). Patients experiencing chronic back pain may also experience high levels of psychological distress associated with material and socio-economic losses (Walker, et al., 2006).

Advancements in medicine and technology in the last decade have increased the life expectancy of humans. It has been estimated by the United Nations that the world population of individuals aged 60 years or older will triple by 2050 (Wong, et al., 2017). The inevitably aging population increases the likelihood of non-communicable diseases such as disc degeneration, disc herniations, and outer annular tears, which all contribute to low-back pain (Battié, et al., 1995; Manchikanti, et al., 2014). It is therefore desirable to develop better and more accessible solutions for pain management given the high cost of surgical treatment and debilitating effects of back pain.

Paper No.xx-xxxx (This paper is based on the paper in the proceedings of xxxxx Conference (20xx), No.xxx.)
[DOI: 10.1299/xxx.20XXxxx000x]

1.2 Existing Treatments

For patients with back pain conditions that do not warrant surgery, interventional pain management therapies are available. One treatment for chronic back pain is an epidural steroid injection (ESI), which is one of the most common procedures used in pain management (Cohen, et al., 2013). In an epidural steroid injection, a medical practitioner injects corticosteroid mixture into the spine to provide temporary relief to patients with herniated discs, arthritis, and other complications (Ackerman and Ahmad, 2007). For well-selected candidates for the procedure, epidural steroid injections provide between 6 weeks and 3 months of relief. However, continuous alleviation of pain requires routine ESI procedures or further treatment, which could include surgery (Cohen, et al., 2013).

Another common procedure in pain management is radiofrequency ablation (RFA), which uses an insulated needle to administer a high frequency current to produce a temperature lesion. The presence of the lesion prevents pain signals from being sent to the brain (Rana, 2013). Radiofrequency ablation can provide pain relief lasting from 6 months to 3 years. Repeated radiofrequency ablation is also performed when symptoms return, with relief provided in 85% of patients up to 10 months (Kennedy, 2019). A drawback to ESI, RFA, and other procedures without a surgical incision is that fluoroscopy is often utilized to determine the position of a medical instrument. This exposes both the patient and the clinicians to ionizing radiation (Kim, et al., 2016). When repeated treatments and visits are necessary such as with an epidural steroid injection, patients are exposed on a continuous basis. Furthermore, surgeons and technicians frequently use fluoroscopy more often during minimally invasive procedures, resulting in increased radiation exposure and subsequent complications (Srinivasan, et al., 2014; Mariscalco, et al., 2011).

A drawback to ESI, RFA, and other procedures without a surgical incision is that fluoroscopy is often utilized to determine the position of a medical instrument. This exposes both the patient and the clinicians to ionizing radiation (Kim, et al., 2016). When repeated treatments and visits are necessary such as with an epidural steroid injection, patients are exposed on a continuous basis. Furthermore, surgeons and technicians frequently use fluoroscopy more often during minimally invasive procedures, resulting in increased radiation exposure and subsequent complications (Srinivasan, et al., 2014; Mariscalco, et al., 2011).

Other techniques for determining the location of a medical instrument include the so-called loss-of-resistance (LOR) technique and ultrasonography. The loss-of-resistance technique involves identifying the spinal epidural space through a loss in physical resistance after penetrating the ligamentum flavum. A study comparing the reliability of the loss-of-resistance technique and fluoroscopy with a 20-gauge Tuohy needle showed that the loss-of-resistance technique was inferior to fluoroscopy. In particular, poor reliability was associated with patients older than 70 years and male patients (Liu, et al., 2001).

Ultrasonography was found to have superior accuracy, improved visualization of anatomy, and absence of ionizing radiation. However, it is limited due to its inability to penetrate dense tissue such as bone structures (Korbe, et al., 2015). Lumbar injections with ultrasonography were found to have poor visibility of the nerve root and neural foramen due to depth and acoustic shadowing artifacts (Narouze and Peng, 2010). Visibility was further obscured in obese patients (Korbe, et al., 2015).

It is evident that an improved and reliable navigation system without ionizing radiation is highly desirable.

1.3 Proposed Technology

In this paper, we investigate a novel 3D navigation system in order to both reduce radiation exposure and improve the accuracy of needle positioning performed by medical practitioners (Vávra, et al., 2017). The new navigation system involves the use of augmented reality and non-invasive skin markers coupled with an MRI scan. A preoperative MRI scan using non-invasive skin markers allows the generation of a 3D model of the patient's body where surgery will be performed. This enables the physician to plan out the surgery in advance, paying special attention to the patient's individualized and unique anatomy. During the procedure, cameras will locate the skin markers on the patient's body and match them up with those in the 3D image, as shown in Fig.1a.

[DOI: 10.1299/xxx.20XXxxx000x]

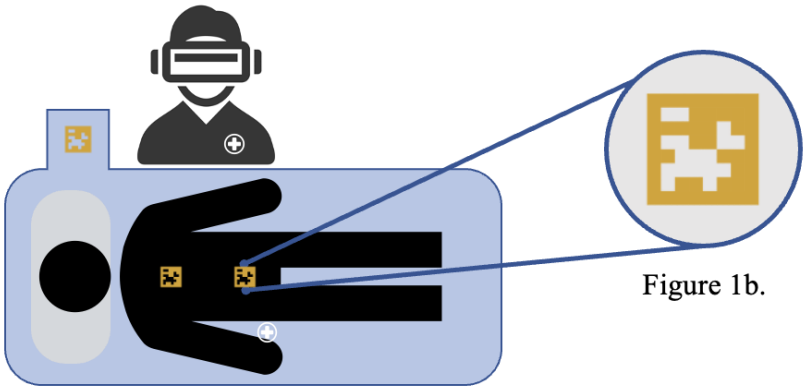

Fig. 1 (a) Diagram of skin markers on the patient and operating room table. (b) close-up view of skin markers.

The physician will then be able to access the 3D model overlaid on top of the patient using an augmented reality headset. The augmented reality system will eliminate the need to periodically view an external screen by providing necessary visual information of the patient through the interfaced MRI image. The goal of the system is to increase the accuracy of surgical operations, reducing operation time on patients, and reducing the number of necessary fluoroscopy scans.

This paper will primarily focus on the development of the marker tracking system in two dimensions using cameras for position detection. Specifically, this paper will cover the accuracy and feasibility of tracking markers in real-time using digital filtering techniques and marker tracking libraries. Open-source markers, known as ArUco markers, will be shuttled around in 2D space at a known speed using a motorized marker platform. The pixel coordinates of the markers will be exported and Kalman filtered. Finally, the measured marker positions will be compared to ground-truth marker platform distances. In a future publication, the development of a 3D marker tracking system and the integration with pre-operative MRI scans will be described.

2. Nomenclature Table

Important symbols are defined as shown below.

x_k	position in the X direction
y_k	position in the Y direction
$\dot{x_k}$	velocity in the X direction
$\dot{y_k}$	velocity in the Y direction
$\ddot{x_k}$	acceleration in the X direction
$\ddot{y_k}$	acceleration in the Y direction
F	state transition matrix
H	observation matrix

3. Development Process

3.1 XYZ Platform

To test the implementation of real-time marker tracking, a testing platform is needed to compare the accuracy of the position tracking algorithm compared to the true position of the marker. To do this, an XYZ platform was built to validate position tracking. Figure 2 shows the computer-aided design of the system, and Fig. 3 shows the constructed XYZ platform.

[DOI: 10.1299/xxx.20XXxxx000x]

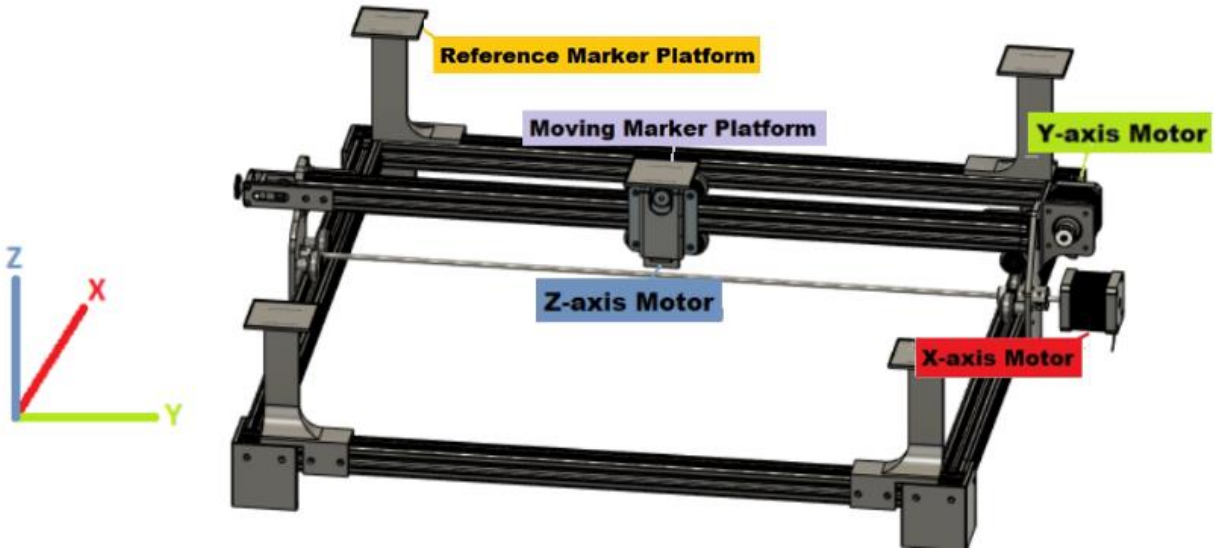

Fig. 2 Computer-aided design model of the XYZ platform. The XYZ platform comes with three stepper motors to move the marker platform in the X, Y, and Z directions. The reference markers are located at the corners of the XYZ platform.

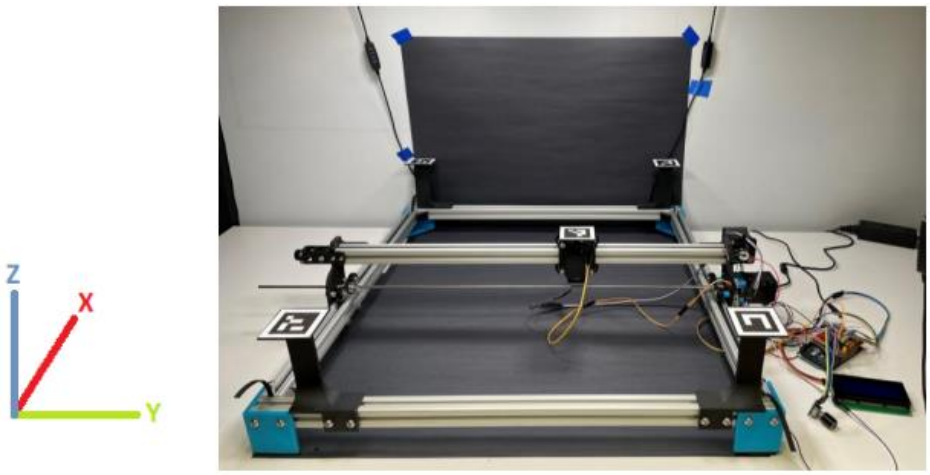

Fig. 3 Physical model of the XYZ platform. The moving marker is able to move in the X, Y, and Z directions. The X, Y, and Z motors are controlled via Arduino microprocessors.

The platform spans 500 mm by 500 mm in the X and Y directions. The movement of the platform is controlled by the X, Y, and Z axis stepper motors, which move the marker platform around. The markers used in the XYZ platform are classified as either moving or reference markers. The reference markers are located on the edges of the platform. The moving marker is located in the center of the platform and is shuttled around by three stepper motors pertaining to the three degrees of freedom.

[DOI: 10.1299/xxx.20XXxxx000x]

3.2 ArUco Markers

The marker tracking implementation makes use of ArUco markers, which are open-source fiducial markers dedicated to positional tracking in real time. Figure 4 shows the details of a typical ArUco marker. The bit grid inside the inner black border of the ArUco marker is used to facilitate marker identification. The outer white margin of the marker is used to separate the marker itself from the background for optimal detection (OpenCV, no date).

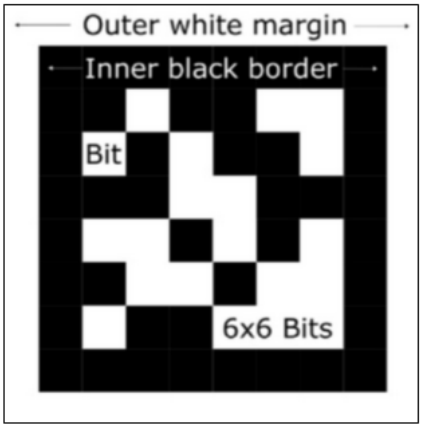

Fig. 4 Typical ArUco code marker. The white bits of information inside the inner black border serve to track the marker ID as the marker moves in real time. The outer white margin is used to provide a visual barrier between the background and the actual marker itself.

The ArUco marker library was utilized to facilitate marker tracking (Garrido-Jurado, et al., 2014). OpenCV was used to interface the markers within Python (OpenCV, no date). This was done by tracking the center pixel coordinates of the markers as they move through space. Thus, the relative position of the moving marker with respect to each of the reference markers can be determined. Since the reference markers are fixed, a world frame of reference is created for analysis from the camera's frame of reference. Table 1 displays the default parameters used in testing. Pixel density refers to the number of bits encoding the marker identification information. For example, in Fig. 4, the pixel density is 6x6 pixels.

Table 1 Default parameters used in marker experiments.

Parameters	Settings
Marker platform speed	10 mm/s
Pixel density	4x4 pixels
Pixel size	4 cm
White border width	1 bit
Camera resolution	1080p
Frames per second	60 fps

In our experiments, video recordings of markers moving on the XYZ platform were taken using a smartphone camera. The camera was calibrated according to ArUco documentation (OpenCV, no date). Videos were processed in Python using OpenCV to give the pixel coordinates of the markers relative to the reference markers.

3.3 Kalman Filtering Implementation

To improve marker tracking, Kalman filtering was implemented in Python as part of post-processing. Kalman filtering is a widely used sensor and data fusion algorithm for dynamic applications. The basic Kalman filter is discrete, recursive, and derives an estimated state of a linear system in real-time. Common applications for Kalman filtering include vehicle navigation, radar sensors, and computer vision measurements. For more complex non-linear applications

[DOI: 10.1299/xxx.20XXxxx000x]

such as satellite navigation, the extended Kalman filter (EKF) is used (Alsadik, 2019).

Other non-linear Kalman filters used for localization, target tracking, and navigation include the unscented Kalman filter, ensemble Kalman filter, and constrained Kalman filter (Ting Goh, et al., 2018). Further applications include the implementation of a linear Kalman filter in object pose tracking with ArUco markers. In applications of marker tracking, linear Kalman filtering was found to reduce tracking noise and was allowed to estimate marker position during temporary instances when the camera was unable to detect markers due to obstructing objects (Kam, et al., 2018).

Our implementation relies on the 2D linear Kalman filter. In 2D Kalman filtering, the kinematic state equations describing the marker tracking system are used.

$$\mathrm{x_k} = \begin{bmatrix} x_k \\ y_k \\ \dot{x}_k \\ \dot{y}_k \end{bmatrix} = \begin{bmatrix} x_k + \dot{x}_{k-1}\Delta\mathrm{t} + \frac{1}{2}\ddot{x}_{k-1}\Delta\mathrm{t}^2 \\ y_k + \dot{y}_{k-1}\Delta\mathrm{t} + \frac{1}{2}\ddot{y}_{k-1}\Delta\mathrm{t}^2 \\ \dot{x}_{k-1} + \ddot{x}_{k-1}\Delta\mathrm{t} \\ \dot{y}_{k-1} + \ddot{y}_{k-1}\Delta\mathrm{t} \end{bmatrix} \tag{1}$$

For our experimental set-up, acceleration is assumed to be negligible since the motors are moving at constant velocity. Thus, the state transition matrix F can be written as

$$F = \begin{bmatrix} 1 & 0 & \Delta\mathrm{t} & 0 \\ 0 & 1 & 0 & \Delta\mathrm{t} \\ 0 & 0 & 1 & 0 \\ 0 & 0 & 0 & 1 \end{bmatrix} \tag{2}$$

The position of the moving marker in the X and Y directions in real-time are the required inputs. Therefore, the observation matrix H can be written as

$$H = \begin{bmatrix} 1 & 0 & 0 & 0 \\ 0 & 1 & 0 & 0 \end{bmatrix} \tag{3}$$

This Kalman filtering implementation was applied to the positional information of the moving marker and implemented using the Pykalman library in Python (pykalman, no date).

3.4 Marker Tracking Implementation

During marker tracking tests, the moving marker was transported around the platform in a square pattern and along the square pattern's diagonals in the X and Y direction. The tracking camera was placed directly above the starting position of the moving marker at a height of 500 mm. Additionally, the camera was placed parallel to the X-Y plane to ensure that only 2D motion was recorded. Figure 5 shows the position of the tracking camera relative to the home position of the moving marker. Figure 6 shows the movement pattern of the marker on the platform. Numbers one through eight correspond to the order of travel.

[DOI: 10.1299/xxx.20XXxxx000x]

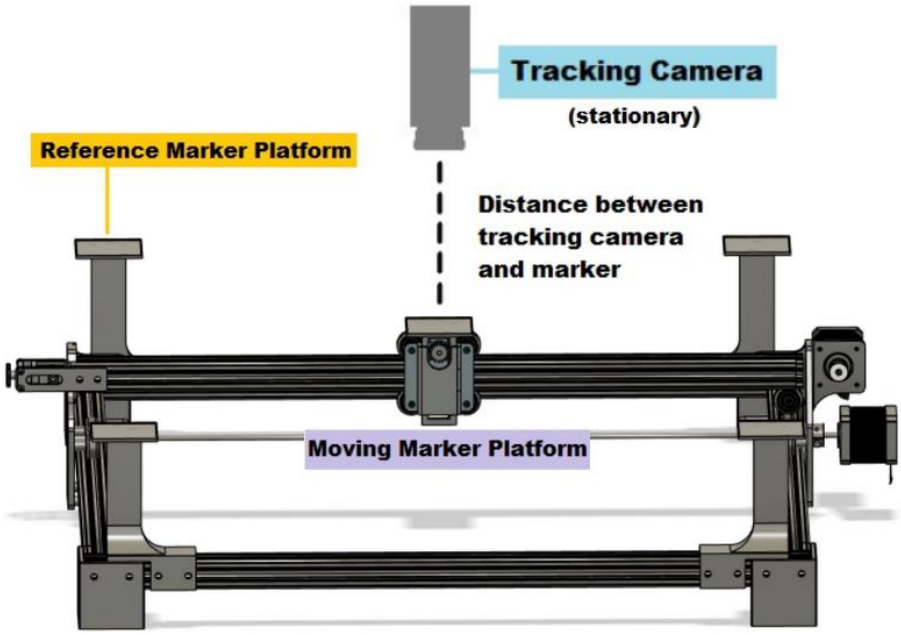

Fig. 5 Tracking camera placed directly above the moving marker at its home position. The camera is placed parallel to the X-Y plane and 500 mm above the moving marker.

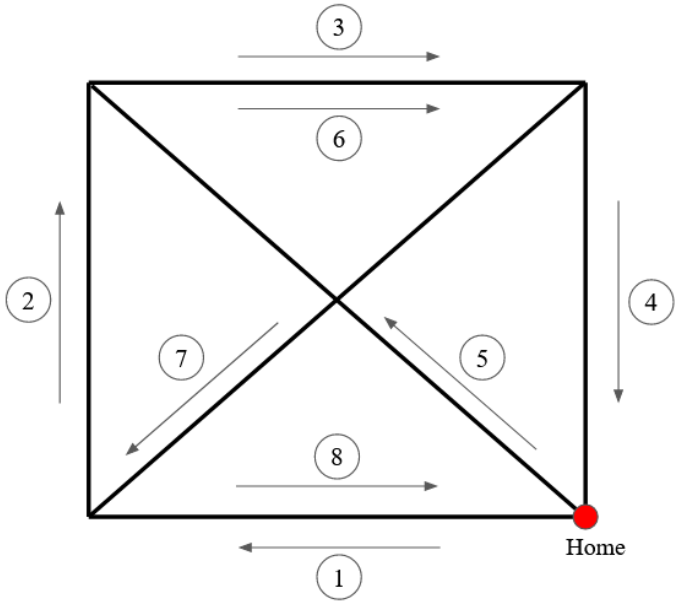

Fig. 6 Marker movement pattern. Numbers one through eight correspond to the order of travel.

Upon capturing the moving marker, the video is transferred into Python for image processing. At each frame, the marker IDs and their center coordinates were captured using built-in ArUco packages in OpenCV. Linear Kalman filtering was then applied to the moving marker. To estimate distance travelled, we converted the pixel position of the markers to position in millimeters using a conversion ratio. The conversion ratio was generated by using the known real-life length of the marker, given to be 40 mm, and dividing it by the pixel length approximated through OpenCV (OpenCV, no date). The pixel length was computed by calculating the Euclidean distance of the marker width.

The details of our marker tracking algorithm are placed in the Appendix.

[DOI: 10.1299/xxx.20XXxxx000x]

4. Results

4.1 XYZ Platform Performance

To account for the positional errors of the platform, the X and Y motors were subject to reset and incremental testing. In reset tests, the moving marker platform was moved 10 mm to 300 mm in increments of 10 mm spacings in the X and Y directions, respectively. In incremental tests, the moving marker was moved in 10 mm increments in the X and Y direction until it reached 300 mm. After each movement, the error was recorded. Three trials were conducted for each test, and the mean error was calculated. Table 2 shows the mean error results in the X and Y directions in the reset test. Table 3 shows the mean error results in the incremental test.

Table 2 Directional mean error in the reset tests.

Direction	Mean Error
X	-0.11 ± 0.07 mm
Y	-0.06 ± 0.09 mm

Table 3 Directional mean error in the incremental tests.

Direction	Mean Error
X	-0.003 ± 0.072 mm
Y	-0.005 ± 0.080 mm

From Table 2, both the X and Y directions appear to underestimate distance. However, from Table 3, there does not appear to be significant underestimating of errors. This suggests that the marker platform performs consistently independently of its location on the X and Y axis.

4.2 Marker Tracking Performance

Following the marker tracking, coordinate data of the moving marker was imported to MATLAB for analysis. The position of the moving marker from the tracking algorithm was compared against the ideal position of the marker associated with the reset tests. The error of the moving marker was plotted as the marker moved through space. Figure 7 displays the error heatmap of the marker moving at 10, 15, and 20 mm/s, respectively. Table 4 shows the error results of the moving marker at 10, 15, and 20 mm/s, respectively, for three trials each.

[DOI: 10.1299/xxx.20XXxxx000x]

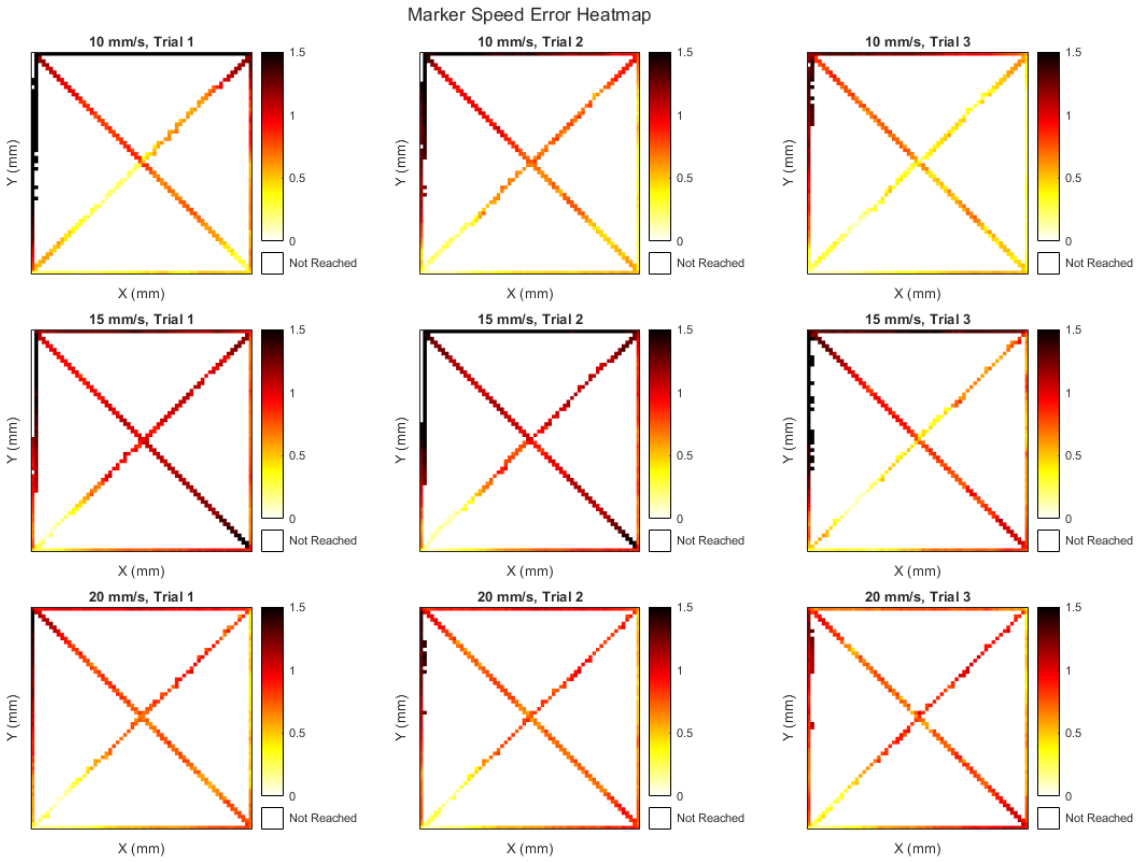

Fig. 7 Plotted coordinates of the marker moving on the testing platform at 10, 15, and 20 mm/s, respectively. Three trials were performed and plotted. Each color corresponds to one movement of the XYZ platform.

Table 4 Moving marker error results at different speeds

Speed (mm/s)	Trial 1 (mm)	Trial 2 (mm)	Trial 3 (mm)
10	1.0 ± 0.7	0.8 ± 0.5	0.7 ± 0.4
15	1.0 ± 0.3	1.1 ± 0.5	0.9 ± 0.5
20	0.7 ± 0.3	0.8 ± 0.3	0.7 ± 0.2

5. Discussion

From Fig. 6, we observe that the largest position error occurs near the back left of the platform in all tests. This is likely due to the fact that the tracking camera is positioned close to the front of the platform. One future consideration to improve positional readings would be to place multiple tracking cameras in the operating room to reduce the distance between cameras and tracked objects. To describe the position of a trackable object, the positional readings of the various cameras could be taken as a weighted average to minimize error. The higher weights could be assigned in terms of which camera was closer to the relevant object being tracked. For instance, the camera closest to the relevant skin marker would be assigned a higher weight than a camera farther away.

For the implementation of a 3D model overlaid on top of a patient, it is important that the error be minimized to avoid positional discrepancies between the generated model and patient anatomy. The maximum error of the moving markers across all trials and platform speeds was approximately 1.5 mm, with the average errors per trial being on the order of 1 mm. These results are acceptable given the low error per trial and the fact that our marker tracking was implemented using only a single camera recording on average video specifications. We estimate that the majority of costs will be from the MRI scans and augmented reality setup, and the cost of the tracking cameras and fiducial markers are almost negligible compared to the other system costs. Thus, the development of the marker tracking system explored

[DOI: 10.1299/xxx.20XXxxx000x]

in this research is very promising due to its very good performance while minimizing costs.

Currently, we are developing a 3D marker tracking system, but this comes with its own challenges. For example, factors such as potential stretching or rotation of markers in space during the tracking will need to be accounted for. After developing the tracking system, fiducial markers must be interfaced with a preoperative MRI scan through augmented reality. In addition, attention needs to be given to marker deformation on the skin to ensure the feasibility of using a 3D map based on an MRI scan. Potential solutions for offsetting the scale of deformation would be to utilize multiple reference markers on the patient, as well as accounting for changes in marker position using tracking software calibration. Software implementations can be tested on artificial tissue samples to simulate the deformations that may occur during clinical studies.

An optimal marker adhesive must be narrowed down through various material tests, such as testing for creep, peel, and durability. The material must also pass cytotoxicity, biocompatibility, and irritation tests to be compatible with human experiments. Additionally, such a marker material should be detectable and trackable by camera software, regardless of potential wear and tear that may occur between the time of an MRI scan and the time of an operation.

In addition to mechanical optimization, anesthesiologists and physicians must be consulted to direct the design and setup of the marker tracking system towards effective usage in the operating room. Factors such as location, size, and quantity of skin markers must be considered.

6. Conclusion

In this study, we explore the possibility of creating an augmented reality system that can be interfaced with MRI to aid in positional tracking of surgical instruments with respect to the surgical field. An XYZ platform was developed in order to conduct ground-truth testing on marker tracking software in 2D. ArUco markers in conjunction with linear Kalman filtering were used in order to track the position of moving markers across the platform. The results show that an augmented reality tracking system with fiducial markers is a promising way for implementation in the operating room.

Future work on this project will address the development of a 3D marker tracking system, as well as further development towards finding optimal marker adhesive materials and integration with preoperative MRI scans. The ultimate goal of the surgical system is to reduce radiation exposure and improve patient outcomes while simultaneously providing a low-cost alternative to existing surgical-assisting technologies used in order to track the position of moving markers across the platform. Although our system was explored for the specific example of needle placement for surgical pain management, the system will be useful for many types of surgery, especially for cases where MRI information supplements surgical procedures.

Acknowledgements

This work was supported in part by a grant from the UCSD General Campus Research Senate #2019201 and the UCSD ACTRI-IEM GEM Grant #1020487.

Appendix

This appendix describes our marker tracking implementation algorithm, which servers to track the marker positions at each frame. Kalman filtering is applied on the moving marker after video processing.

[DOI: 10.1299/xxx.20XXxxx000x]

Algorithm 1 Marker Tracking Implementation

function tracking(video, transition_matrix, state_matrix)
Input : Video recording of marker tracking. Transition and state matrices transition_matrix and state_matrix.
Output : Filtered marker coordinates and IDs.
1: for each video frame **do**
2: **for** markers seen **do**
3: record marker ID
4: record corner coordinates of marker
5: calculate and record the center coordinate using the corner coordinates
6: **end for**
7: end for
8: implement Kalman filter given parameters transition_matrix and state_matrix
9: compute the Euclidean distance of marker width
10: convert Kalman filtered pixel coordinates to millimeters
11: return marker coordinates and IDs

References

Ackerman, W.E. and Ahmad, M., 'The efficacy of lumbar epidural steroid injections in patients with lumbar disc herniations', *Anesthesia and Analgesia*, Vol.104, No.5 (2007), pp.1217–1222.

Alsadik, B., 'Chapter 10 - Kalman Filter', in B. Alsadik (ed.) *Adjustment Models in 3D Geomatics and Computational Geophysics*. Elsevier (Computational Geophysics) (2019), pp.299–326.

Battié, M.C. *et al.*, '1995 Volvo Award in clinical sciences. Determinants of lumbar disc degeneration. A study relating lifetime exposures and magnetic resonance imaging findings in identical twins', *Spine*, Vol.20, No.24 (1995), pp.2601–2612.

Cohen, S.P. *et al.*, 'Epidural steroids: a comprehensive, evidence-based review', *Regional Anesthesia and Pain Medicine*, Vol.38, No.3 (2013), pp.175–200.

Croft, P.R. *et al.*, 'Psychologic distress and low back pain. Evidence from a prospective study in the general population', *Spine*, Vol.20, No.24 (1995), pp.2731–2737.

Currie, S.R. and Wang, J., 'More data on major depression as an antecedent risk factor for first onset of chronic back pain', *Psychological Medicine*, Vol.35, No.9 (2005), pp.1275–1282.

Garrido-Jurado, S. *et al.*, 'Automatic generation and detection of highly reliable fiducial markers under occlusion', *Pattern Recognition*, Vol.47, No.6 (2014), pp.2280–2292.

James, S.L. *et al.* 'Global, regional, and national incidence, prevalence, and years lived with disability for 354 diseases and injuries for 195 countries and territories, 1990–2017: a systematic analysis for the Global Burden of Disease Study 2017', *The Lancet*, Vol.392, No.10159 (2018), pp.1789–1858.

Kam, H.C., Yu, Y.K. and Wong, K.H., 'An Improvement on ArUco Marker for Pose Tracking Using Kalman Filter', in *2018 19th IEEE/ACIS International Conference on Software Engineering, Artificial Intelligence, Networking and Parallel/Distributed Computing (SNPD). 2018 19th IEEE/ACIS International Conference on Software Engineering, Artificial Intelligence, Networking and Parallel/Distributed Computing (SNPD)* (2018), pp.65–69.

Kennedy, D., *Radiofrequency Ablation (RFA) for Facet and Sacroiliac Joint Pain, Spine-health* (no date), available from <https://www.spine-health.com/treatment/injections/radiofrequency-ablation-rfa-facet-and-sacroiliac-joint-pain>, (accessed on 26 November, 2021).

Kim, S. *et al.*, 'Factors Affecting Radiation Exposure during Lumbar Epidural Steroid Injection: A Prospective Study in 759 Patients', *Korean Journal of Radiology*, Vol.17, No.3 (2016), pp. 405–412.

[DOI: 10.1299/xxx.20XXxxx000x]

Korbe, S. *et al.*, 'Ultrasound-guided interventional procedures for chronic pain management', *Pain Management*, Vol.5, No.6 (2015), pp.465–482.

Kovacs, F. *et al.*, 'The Influence of Psychological Factors on Low Back Pain-Related Disability in Community Dwelling Older Persons', *Pain Medicine*, Vol.9 No.7 (2008), pp.871–880.

Liu, S.S. *et al.*, 'Prospective experience with a 20-gauge Tuohy needle for lumbar epidural steroid injections: Is confirmation with fluoroscopy necessary?', *Regional Anesthesia and Pain Medicine*, Vol.26, No.2 (2001), pp.143–146.

Lovo, E.E. *et al.*, 'A novel, inexpensive method of image coregistration for applications in image-guided surgery using augmented reality', *Neurosurgery*, Vol.60, No.4 (Suppl 2) (2007), pp.366–371; discussion 371-372.

Manchikanti, L. *et al.*, 'Epidemiology of Low Back Pain in Adults', *Neuromodulation: Technology at the Neural Interface*, Vol.17 (2014), pp.3–10.

Mariscalco, M.W. *et al.*, 'Radiation exposure to the surgeon during open lumbar microdiscectomy and minimally invasive microdiscectomy: a prospective, controlled trial', *Spine*, Vol.36, No.3 (2011), pp.255–260.

Narouze, S. and Peng, P.W.H., 'Ultrasound-guided interventional procedures in pain medicine: a review of anatomy, sonoanatomy, and procedures. Part II: axial structures', *Regional Anesthesia and Pain Medicine*, Vol.35, No.4 (2010), pp.386–396.

OpenCV: ArUco marker detection (aruco module) (no date), available from <https://docs.opencv.org/4.x/d9/d6d/tutorial_table_of_content_aruco.html>, (accessed on 16 February 2022).

pykalman — pykalman 0.9.2 documentation (2012), available from <https://pykalman.github.io/>, (accessed on 3 July 2022).

Rana, M.V., 'Radiofrequency: Conventional and Pulsed', in T.R. Deer et al. (eds) *Comprehensive Treatment of Chronic Pain by Medical, Interventional, and Integrative Approaches*. New York, NY: Springer New York (2013), pp.285–296.

Sizer, P.S., Matthijs, O. and Phelps, V., 'Influence of age on the development of pathology', *Current Review of Pain*, Vol.4, No.5 (2000), pp.362–373.

Srinivasan, D. *et al.*, 'Radiation safety and spine surgery: systematic review of exposure limits and methods to minimize radiation exposure', *World Neurosurgery*, Vol.82, No.6 (2014), pp.1337–1343.

Ting Goh, S., (Reza) Zekavat, S.A. and Abdelkhalik, O., 'An Introduction to Kalman Filtering Implementation for Localization and Tracking Applications', in *Handbook of Position Location*. John Wiley & Sons, Ltd (2018), pp.143–195.

Truchon, M. *et al.*, 'Low-back-pain related disability: An integration of psychological risk factors into the stress process model', *Pain*, Vol.137, No.3 (2008), pp.564–573.

Vávra, P. *et al.*, 'Recent Development of Augmented Reality in Surgery: A Review', *Journal of Healthcare Engineering* (2017), pp.1–9.

Walker, J., Sofaer, B. and Holloway, I., 'The experience of chronic back pain: Accounts of loss in those seeking help from pain clinics', *European Journal of Pain*, Vol.10, No.3 (2006), pp.199–199.

Wong, A.Y., Karppinen, J. and Samartzis, D., 'Low back pain in older adults: risk factors, management options and future directions', *Scoliosis and Spinal Disorders*, Vol.12, No.14 (2017).

[DOI: 10.1299/xxx.20XXxxx000x]